Journal of Power Sources 268 (2014) 349–355

Contents lists available at ScienceDirect

Journal of Power Sources

journal homepage: www.elsevier.com/locate/jpowsour

Effects of inorganic salts on the morphological, structural, and electrochemical properties of prepared nickel-rich $Li[Ni_{0.6}Co_{0.2}Mn_{0.2}]O_2$

Ki Jae Kim, Yong Nam Jo, Won Jong Lee, T. Subburaj, K. Prasanna, Chang Woo Lee*

Department of Chemical Engineering, College of Engineering, Kyung Hee University, 1732 Deogyeong-daero, Gihung, Yongin, Gyeonggi 446-701, South Korea

HIGHLIGHTS

- Choosing inorganic salts plays a critical role in electrochemical performances.
- $Li[Ni_{0.6}Co_{0.2}Mn_{0.2}]O_2$ is synthesized using various inorganic salts.
- Sulfate induces a large amount of void channel over the secondary particles.
- $Li[Ni_{0.6}Co_{0.2}Mn_{0.2}]O_2$ material by sulfate shows the best cycling performances.

ARTICLE INFO

Article history:
Received 17 April 2014
Received in revised form
10 June 2014
Accepted 10 June 2014
Available online 18 June 2014

Keywords:
Lithium ion battery
Inorganic salts
Nickel-rich
Void channel
High power density

ABSTRACT

The cathode active materials $Li[Ni_{0.6}Co_{0.2}Mn_{0.2}]O_2$ are synthesized using different inorganic salts, sulfate [$NiSO_4 \cdot 6H_2O$, $CoSO_4 \cdot 7H_2O$, $MnSO_4 \cdot H_2O$], nitrate [$M(NO_3)_2 \cdot 6H_2O$ (M = Ni, Co, Mn)] and acetate [$M(CH_3COO)_2 \cdot 4H_2O$ (M = Ni, Co, Mn)]. The X-ray diffraction (XRD) patterns indicate that sulfate and nitrate starting materials formed a well-ordered hexagonal α-$NaFeO_2$ layered structure (space group: 166, $R\bar{3}m$). However, acetate starting material is led to a poorly layered structure compared to the other materials. Field emission scanning electron microscope (FE-SEM) images show that sulfate and acetate starting materials formed nano-sized primary particles with a size of about 200–500 nm and 300 nm, and void channels. However, the primary particles with a size of 300 nm from nitrate starting material agglomerate together to form micro-sized secondary particles. The initial discharge capacities of the sulfate, nitrate, and acetate starting materials are 138.3, 142.4, and 135.9 mAh g^{-1} at 1 C-rate in the voltage range 3.0–4.3 V vs. Li/Li^+, respectively. The discharge capacity retentions of sulfate, nitrate, and acetate starting materials are 92.5%, 63.9%, and 78.1% at 1 C-rate after 50 cycles, and 83.2%, 48.0%, and 71.7% at 6 C-rate after 100 cycles, respectively.

1. Introduction

Rechargeable lithium ion batteries have been widely investigated as power sources for electronic devices such as cellular phones and laptop computers. Furthermore, higher energy density, longer cycle life, and better safety are necessary battery improvements for the development of hybrid electric vehicle (HEV), plug in hybrid electric vehicle (P-HEV), zero-emission electric vehicle (EV), and energy storage system (ESS), which can accumulate a large amount of the energy generated from wind power and solar cell plants [1–5].

In the last few years, lithium cobalt oxide has been widely used and investigated as a cathode active material because of its high coefficient of lithium ion diffusion and ease of processing. However, lithium cobalt oxide has several disadvantages such as toxicity, high cost, and poor rate capability. In addition, high energy and power density are required for large-scaled devices like EVs and ESS. Thus, many research groups have focused on finding new cathode materials that can provide high power and energy density for lithium ion batteries [6–8].

Among existing cathode materials, Ni-rich materials, $Li[Ni_{1-x-y}Co_xMn_y]O_2$ $(1-x-y \geq 0.5)$, are the most promising candidates for applications of EVs and ESS due to their excellent cycling ability, high specific capacity, relatively low toxicity, and good rate capability [9–12]. There are various inorganic synthesis methods such as the sol–gel process, hydrothermal synthesis, solid state reactions, and

* Corresponding author. Tel.: +82 31 201 3825; fax: +82 31 204 8114.
E-mail address: cwlee@khu.ac.kr (C.W. Lee).

http://dx.doi.org/10.1016/j.jpowsour.2014.06.057
0378-7753/

co-precipitation to prepare Ni-rich cathode materials [32,33]. Among these methods, co-precipitation has been widely used because it allows the uniform and homogeneous distribution of elements in particles and materials can be prepared on a large scale [13–18]. In co-precipitation, there are many factors that affect the physical properties of the product such as pH, temperature, agitation velocity, shape of reactor, feed rate, and starting materials, since the complex reactions are affected by various conditions that form the stabilized product [34]. In particular, anions of inorganic salts have an effect on the morphological and structural properties by changing the zeta potential and atmosphere of particles in solution [19–21].

In this study, $Li[Ni_{0.6}Co_{0.2}Mn_{0.2}]O_2$ cathode materials are synthesized by the co-precipitation method. The effects of different inorganic salt starting materials such as sulfate, nitrate, and acetate compounds on the morphological, structural, and electrochemical properties of the product $Li[Ni_{0.6}Co_{0.2}Mn_{0.2}]O_2$ were investigated.

2. Experimental

2.1. Synthesis of $Li[Ni_{0.6}Co_{0.2}Mn_{0.2}]O_2$

The $Ni_{0.6}Co_{0.2}Mn_{0.2}(OH)_2$ precursor was synthesized by co-precipitation in the following manner. Three inorganic salts, sulfate [$NiSO_4 \cdot 6H_2O$, $CoSO_4 \cdot 7H_2O$, $MnSO_4 \cdot H_2O$], acetate [$M(CH_3COO)_2 \cdot 4H_2O$ (M = Ni,Co,Mn)], and nitrate [$M(NO_3)_2 \cdot 6H_2O$ (M = Ni, Co, Mn)], were employed. First, the metal salts (mol.% of Ni:Co:Mn = 6:2:2) were dissolved in distilled water with a total concentration of 2 mol L^{-1}, and the solution was pumped into a continuously stirred tank reactor. 4 mol L^{-1} NaOH and 1 mol L^{-1} NH_4OH solutions were simultaneously fed into the reactor. The solution was maintained at 50 °C under vigorous stirring for 12 h, and the pH value (pH = 11.0 ± 0.2) of the solution in the reactor was carefully controlled by the rate of NaOH addition. After the reaction, the precursor $Ni_{0.6}Co_{0.2}Mn_{0.2}(OH)_2$ was filtered, thoroughly washed, and then dried at 110 °C for 5 h. The obtained precursor was mixed with excess LiOH (mol.% of Mn + Co + Ni):Li = 1:1.05) to account for evaporation of lithium at high temperature. Finally, the mixture was sintered at 470 °C for 5 h and calcined at 850 °C for 5 h in air at a heating rate of 5 °C min^{-1}.

2.2. Preparation of the 2032 type coin cell

For fabrication of cathode electrodes, the obtained cathode active material, $Li[Ni_{0.6}Co_{0.2}Mn_{0.2}]O_2$ powder, was mixed with carbon black and polyvinylidene difluoride (PVdF) in wt.% of 85:7.5:7.5 in N-methyl-2-pyrrolidone solvent. The obtained slurry was laminated on Al foil and then dried at 120 °C for 5 h. A 2032 type coin cell was fabricated as a half-cell system using the obtained electrode as the cathode and lithium metal as the anode. A Celgard 3501 microporous membrane was used as a separator, and the electrolyte was 1.15 M $LiPF_6$ in ethylene carbonate:ethyl methyl carbonate = 3:7 vol.%.

Table 1
Structural parameters of $Li[Ni_{0.6}Co_{0.2}Mn_{0.2}]O_2$ samples made by different inorganic salts.

Samples	a (Å)	c (Å)	c/a	Volume (Å^3)	I_{003}/I_{104}[a]
Sulfate	2.8735	14.2198	4.9486	101.6812	1.5936
Nitrate	2.8684	14.2043	4.9520	101.2142	1.5012
Acetate	2.8697	14.2239	4.9566	101.4421	1.2757

[a] I_{003}/I_{104} is the ratio of the intensities of the (003) and (104) peaks.

2.3. Characterization

The crystalline structure of prepared powders was analyzed by XRD (D8 Advance, Bruker) employing Cu Kα radiation. XRD data were obtained at $2\theta = 10°–80°$ with a step size of 0.02°. The TOPAS Rietveld program was applied to analyze the powder diffraction patterns. The stoichiometric ratio at the powder surface was determined using X-ray photoelectron spectroscopy (XPS, K-Alpha, Thermo Electron). Surface morphology and particle size were observed using FE-SEM (Leo Supra 55, Carl Zeiss). Elemental composition was determined by inductively coupled plasma optical emission spectroscopy (ICP-OES, Direct Reading Echelle ICP, Leeman).

Cycling performance of cathode material $Li[Ni_{0.6}Co_{0.2}Mn_{0.2}]O_2$ was evaluated in the range of 3.0–4.3 V in constant-current and constant-voltage mode using a battery cycler (BT-2000, Arbin). AC impedance measurements were performed using an electrochemical analyzer (Iviumstat, Ivium Technologies) over the frequency range of 1 mHz–100 kHz with an amplitude of 10 mV. Cyclic voltammetry (CV) was performed using an electrochemical analyzer (Iviumstat, Ivium Technologies) over 3.0–4.5 V at a scanning rate 0.1 mV s^{-1}.

3. Results and discussion

The XRD patterns for prepared $Ni_{0.6}Co_{0.2}Mn_{0.2}(OH)_2$ and $Li[Ni_{0.6}Co_{0.2}Mn_{0.2}]O_2$ with different sulfate, nitrate, and acetate

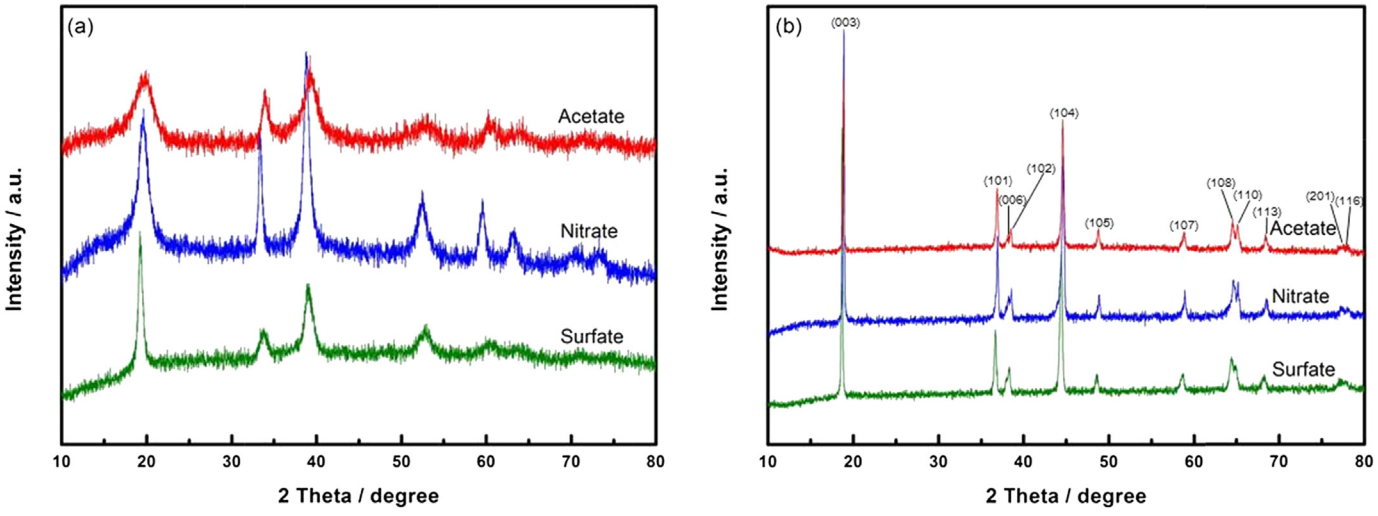

Fig. 1. XRD patterns of (a) $Ni_{0.6}Co_{0.2}Mn_{0.2}(OH)_2$ precursor samples and (b) $Li[Ni_{0.6}Co_{0.2}Mn_{0.2}]O_2$ calcined samples.

Table 2
ICP data of all samples made by different inorganic salts.

Inorganic salt	Element	ppm (1)	ppm (2)	ppm (3)	ppm avg.	Molar ratio
Sulfate	Ni	6.80	6.79	6.76	6.78	0.576
	Co	2.65	2.68	2.72	2.68	0.227
	Mn	2.18	2.13	2.19	2.17	0.197
Nitrate	Ni	4.25	4.21	4.23	4.23	0.572
	Co	1.59	1.55	1.51	1.55	0.210
	Mn	1.58	1.62	1.63	1.61	0.218
Acetate	Ni	3.73	3.77	3.78	3.76	0.556
	Co	1.45	1.49	1.47	1.47	0.216
	Mn	1.45	1.44	1.44	1.44	0.228

inorganic salts as starting materials are shown in Fig. 1. Hereafter, the materials synthesized using these different inorganic salt starting materials are referred to as Sulfate, Nitrate, and Acetate. Before calcination, peaks of Sulfate and Nitrate were sharper than those of Acetate, which indicated that Sulfate and Nitrate gave well-ordered metal hydroxide compared to Acetate. After calcination, XRD patterns of Sulfate, Nitrate, and Acetate corresponded to a hexagonal α-$NaFeO_2$ layered structure. And the elemental compositions of the obtained Sulfate, Nitrate and Acetate were determined as shown in Table 2. In the XRD patterns, the intensity ratio of the (003)/(104) peaks and the splitting of the (006), (102) peaks and (018), (110) peaks were indications of materials with characteristic layered structures [1,22]. In particular, it is known that the intensity ratio of the (003)/(104) peaks depend on the degree of displacement between ions located at the 3a (Li layers) and 3b (transition metal layers) sites in the $R\bar{3}m$ space group. Undesirable cation mixing would take place when the intensity ratio of the (003)/(104) peaks was less than 1.2 [23]. Table 1 summarizes the estimated structural parameters of the Sulfate, Nitrate and Acetate products. The unit cell volumes of Sulfate, Nitrate and Acetate were 101.68, 101.21, and 101.44, respectively. The intensity ratio at >1.2 of the (003)/(104) diffraction peaks from all of the powders indicated excellent cation ordering. Among these materials, it was clear that Sulfate had minimal cation mixing, which could lead to excellent electrochemical performances.

FE-SEM images of prepared $Ni_{0.6}Co_{0.2}Mn_{0.2}(OH)_2$ and $Li[Ni_{0.6}Co_{0.2}Mn_{0.2}]O_2$ from Sulfate, Nitrate, and Acetate are shown in Fig. 2. In the case of Sulfate, many scattered flakes were observed as shown in Fig. 2(a). After calcination, primary particles with an approximate size of 200–500 nm were formed, and many void channels were observed as seen in Fig. 2(b). In the case of Nitrate, some agglomerated flakes were observed as shown in Fig. 2(c). After calcination, micro-sized secondary particles were formed by

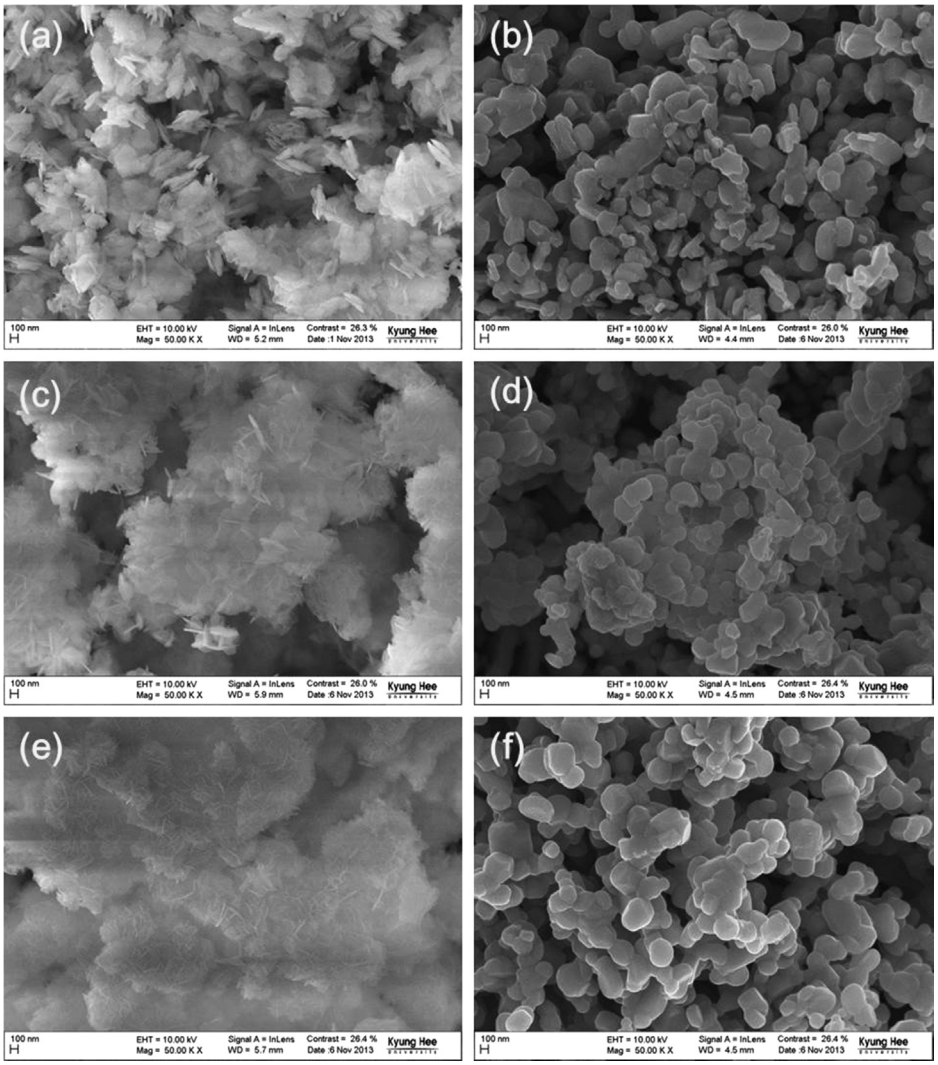

Fig. 2. FE-SEM images of $Ni_{0.6}Co_{0.2}Mn_{0.2}(OH)_2$ precursor samples (a) Sulfate (c) Nitrate (e) Acetate and $Li[Ni_{0.6}Co_{0.2}Mn_{0.2}]O_2$ calcined samples (b) Sulfate (d) Nitrate (f) Acetate.

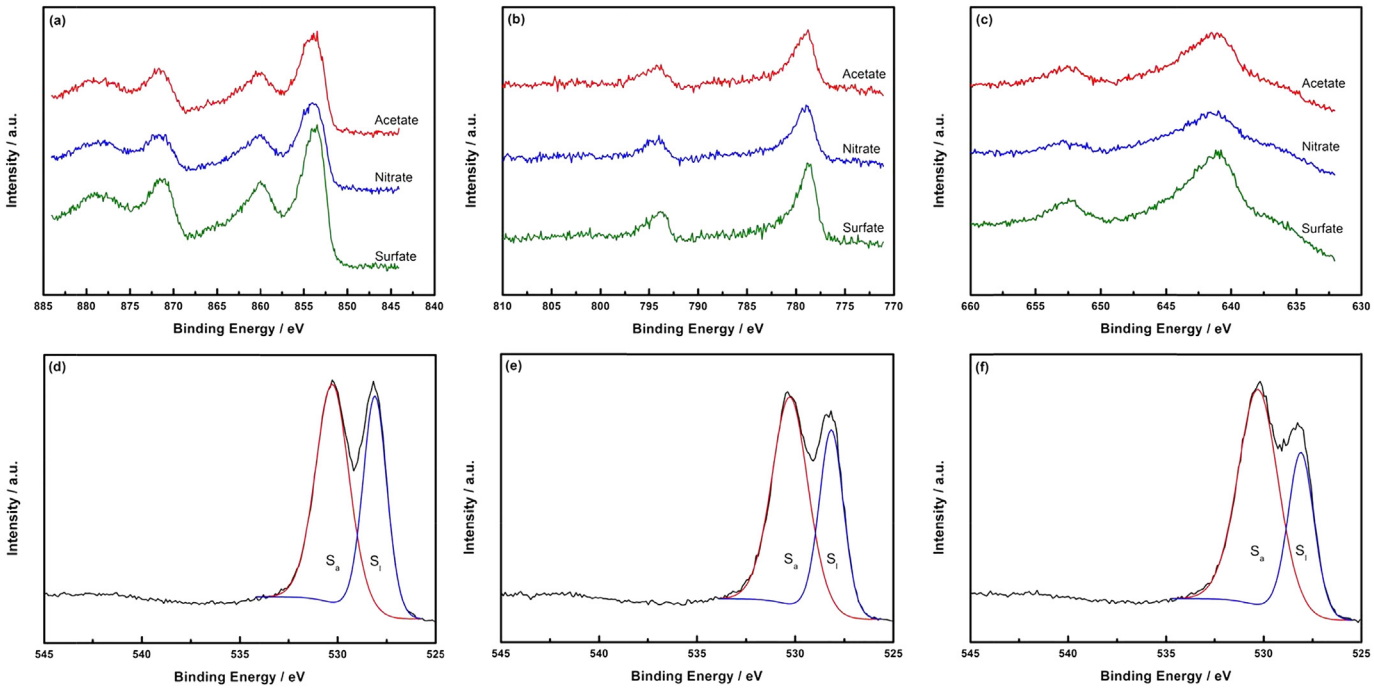

Fig. 3. XPS spectra of (a) Ni 2p, (b) Co 2p, (c) Mn 2p, (d) O 1s of Sulfate (e) O 1s of Nitrate and (f) O 1s of Acetate for $Li[Ni_{0.6}Co_{0.2}Mn_{0.2}]O_2$ samples.

agglomeration of many primary particles with a size of about 300 nm as shown in Fig. 2(d). In the case of Acetate, agglomerated amorphous clusters were observed as shown in Fig. 2(e). After calcination, primary particles with a size of about 300 nm and void channels were formed by agglomeration of primary particles as shown in Fig. 2(f).

XPS spectra of the Ni 2p, Co 2p, Mn 2p, and O 1s for $Li[Ni_{0.6}Co_{0.2}Mn_{0.2}]O_2$ powder synthesized using Sulfate, Nitrate, and Acetate are shown in Fig. 3. All of the Ni $2p_{3/2}$, Co $2p_{3/2}$, and Mn $2p_{3/2}$ peaks of the powders were located around 641.5 eV, 778 eV, and 854 eV, similar to the binding energies of Ni^{2+} in NiO (853.8 eV), $Co^{2+/3+}$ in Co_3O_4 (778.4 eV), and Mn^{4+} in β-MnO_2 (641.1 eV), respectively. These data indicate that Ni, Co, and Mn exist as Ni^{2+}, $Co^{2+/3+}$, and Mn^{4+} in the $Li[Ni_{0.6}Co_{0.2}Mn_{0.2}]O_2$ powders [24,25]. The O 1s peak at approximately 529 eV corresponds to lattice oxygens. Another O 1s peak at approximately 531 eV corresponds to absorbed oxygen, which comes from surface CO_3^{2-}, −OH, and impurities from air exposed $LiMO_2$ materials, resulting from adsorption of CO_2 and water under reagent storage conditions [26,27]. The S_a/S_l ratio of the O 1s peak area, which was highly variable in both peak shape and intensity depending on the inorganic starting materials, was found to be 1.402, 1.664, and 2.034 for Sulfate, Nitrate, and Acetate, respectively (S_a: absorbed oxygen, S_l: latticed oxygen). Sulfate had the lowest amount of surface CO_3^{2-} and −OH impurities, and Acetate had the largest amount of impurities on the surface, which can be attributed to chemical stabilization during the synthesis and storage conditions. Sulfate starting materials could form $Li[Ni_{0.6}Co_{0.2}Mn_{0.2}]O_2$ of uniform composition and purity via its stable structure corresponding to the XRD results.

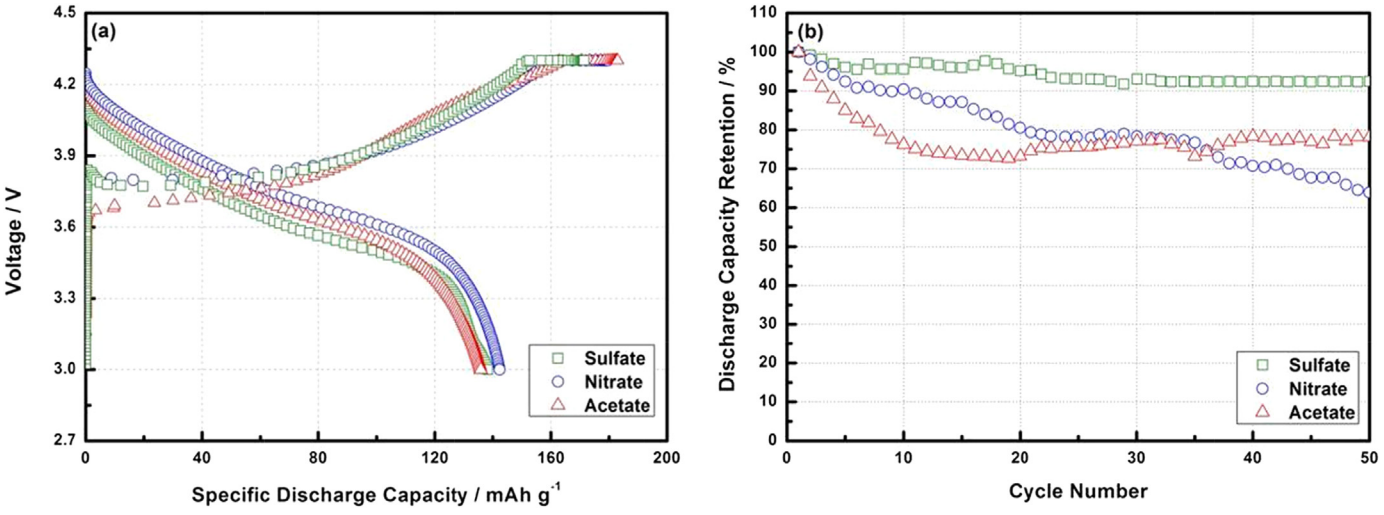

Fig. 4. (a) Initial charge–discharge curves and (b) Discharge capacity retention at 1 C-rate for $Li[Ni_{0.6}Co_{0.2}Mn_{0.2}]O_2$ samples.

Fig. 4(a) shows initial charge–discharge curves for Sulfate, Nitrate and Acetate in the range of 3.0–4.3 V at 1 C-rate. The initial specific discharge capacities were found to be 138.3, 142.4, and 135.9 mAh g^{-1} with a relatively lower coulombic efficiency of 80.70%, 79.34% and 74.32%, respectively as shown in Fig. 4(a). The lowest coulombic efficiency of Acetate can be attributed to much undesirable cation mixing, which can make an irreversible compound corresponding to the XRD result. The discharge capacity retention reached 97.5%, 79.8%, and 63.3% after 50 cycles for Sulfate, Nitrate and Acetate, respectively, as shown in Fig. 4(b). Although Nitrate exhibited the highest first discharge capacity, the retention of discharge capacity continued to decrease and became the lowest after 50 cycles. On the other hand, the discharge capacity retention of Sulfate and Acetate stabilized after 20 cycles and was maintained up to 50 cycles.

In order to observe the cycling stability at a high current rate for power density, electrochemical performance at 6 C-rate was investigated. The discharge capacity retention of Nitrate continued to decrease during cycling, and only 48.0% of its initial capacity remained after 100 cycles. However, Sulfate showed a gradual capacity fading up to 40 cycles and then it became stable maintaining at 83.2% up to 100 cycles whereas Acetate showed a fast capacity fading in the initial 10 cycles and then stably maintained at 71.7% up to 100 cycles as shown in Fig. 5(a). The cyclic voltammograms for Sulfate, Nitrate, and Acetate at 6 C-rate are shown in Fig. 5(b), (c), and (d). All three samples exhibited a typical curve shape composed of reduction peaks centered at 3.5–3.8 V. The oxidation of $Ni^{2+}/^{4+}$ occurs at approximately 3.7 V, and the voltage difference between anodic and cathodic peaks increases as the reversibility of the electrode reaction decreases. Furthermore, the intensity of the anodic and cathodic peaks gradually decreases according to the changing rate as products become unstable and transform into irreversible materials [28,29]. The intensity of the Sulfate reduction peak decreased slightly over the initial 20 cycles and then almost did not change up to 100 cycles as shown in Fig. 5(b). With Acetate, the reduction peak dramatically decreased during the initial 20 cycles, but was essentially stable up to 100 cycles as shown in Fig. 5(d), and Nitrate continued to decrease over 100 cycles as shown in Fig. 5(c).

Electrochemical impedance spectroscopy is a powerful tool for probing the kinetics of lithium intercalation/deintercalation into electrodes. To understand the electrochemical behavior of the electrode reaction corresponding to physical properties, the ac impedance of cells fabricated from Sulfate, Nitrate, and Acetate was measured under conditions of 6 C-rate at 1, 20, and 100 cycles, and the results are shown in Fig. 6. Because the ac impedance behavior of the cell depends on the state of charge (SoC), ac impedance spectra were measured at a SoC of 100 to observe the electrode reaction at the cathode. In ac impedance spectra from all of the materials, two overlapping semicircles were observed. The semicircle in the high frequency range can be attributed to

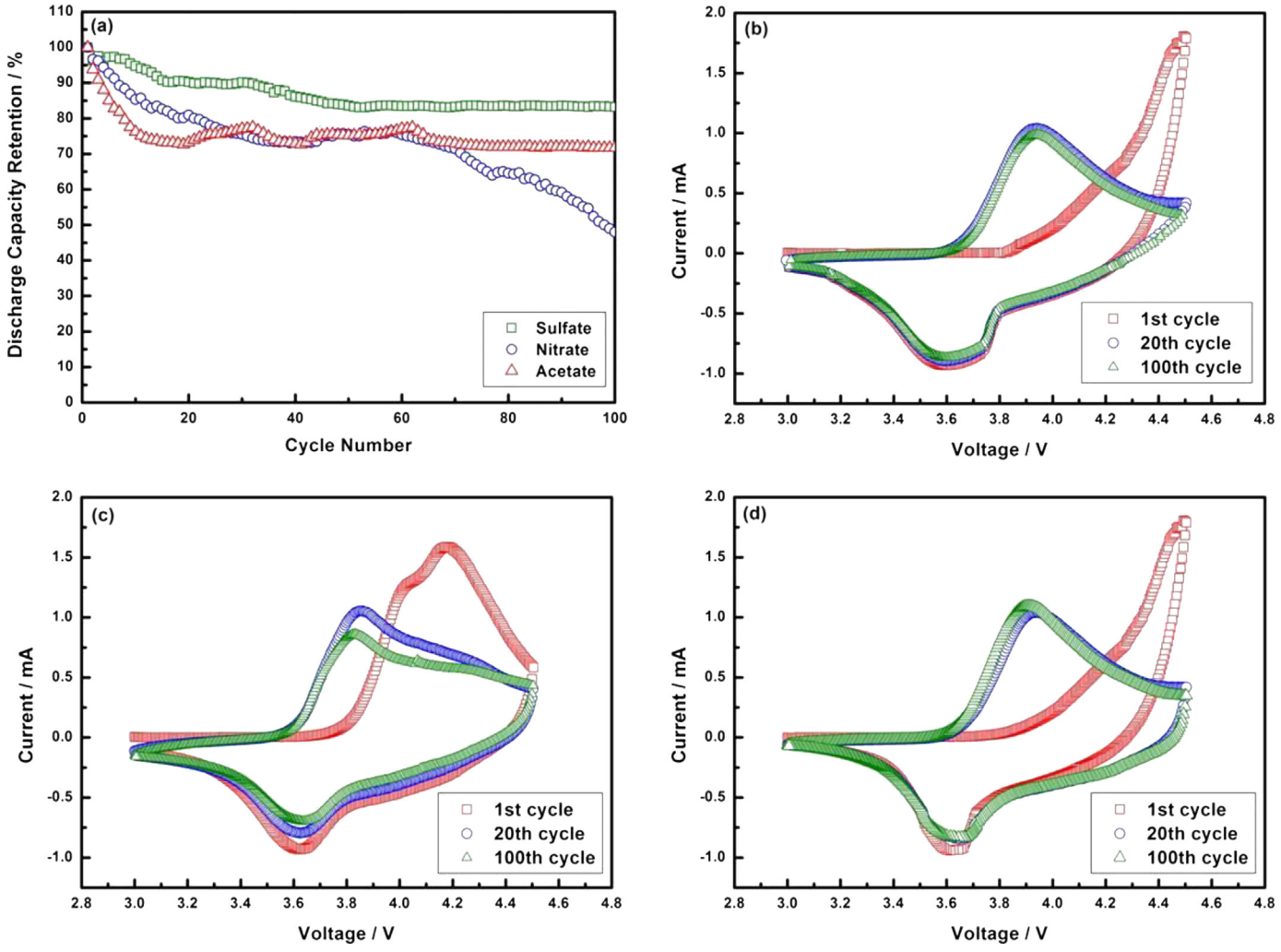

Fig. 5. (a) Discharge capacity retention and cyclic voltammograms of (b) Sulfate, (c) Nitrate and (d) Acetate at 6 C-rate for $Li[Ni_{0.6}Co_{0.2}Mn_{0.2}]O_2$ samples.

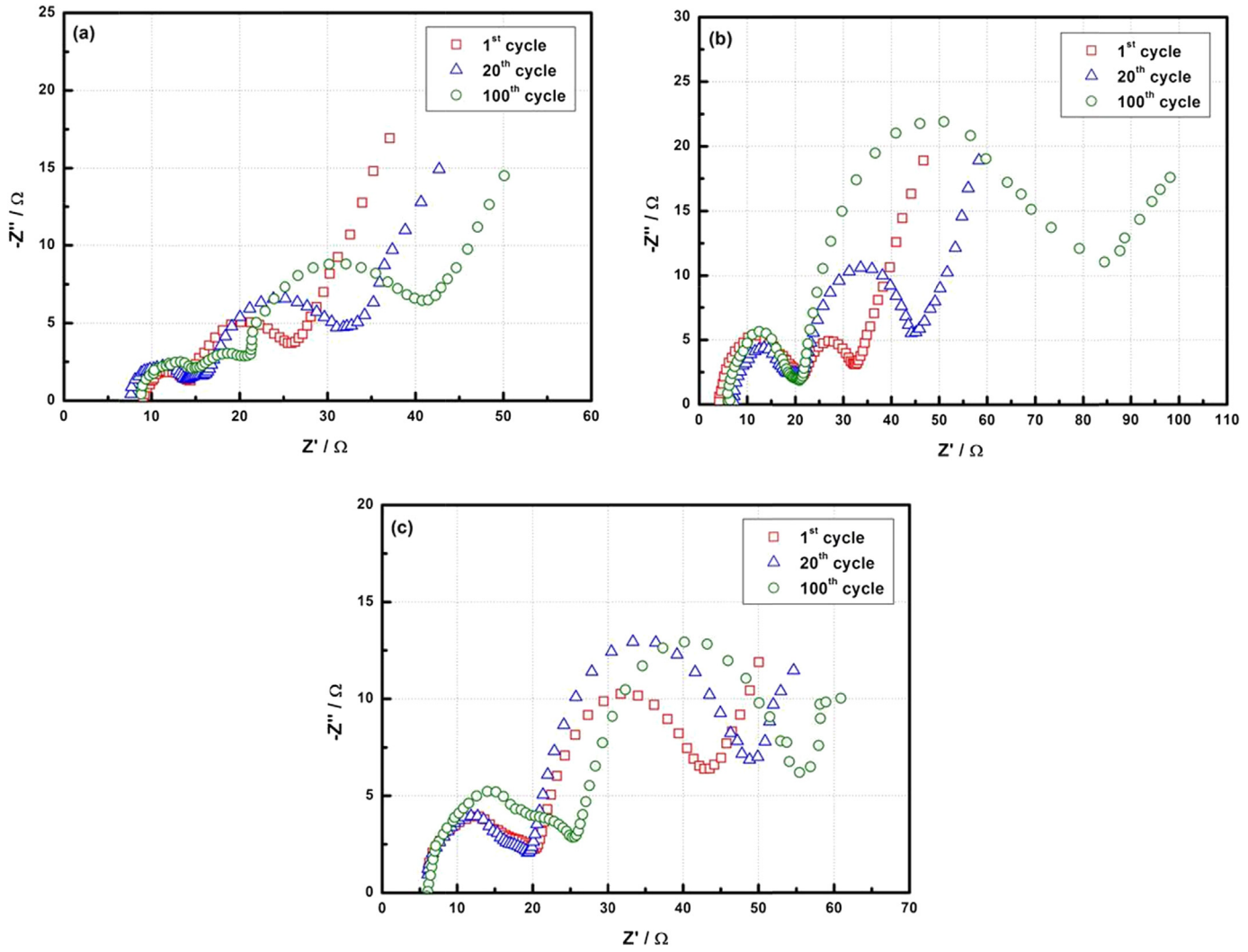

Fig. 6. AC impedance spectra obtained at 4.3 V charged state of (a) Sulfate, (b) Nitrate and (c) Acetate after 1 cycle, 20 cycles and 100 cycles at 6 C-rate for $Li[Ni_{0.6}Co_{0.2}Mn_{0.2}]O_2$ samples.

resistance of Li^+ ion migration through the solid electrolyte interphase layer of the electrode (R_f), while the semicircle in the low-middle frequency range is due to charge transfer resistance between the electrode and electrolyte (R_{ct}) [30]. For all of the materials, the impedance of the high-frequency process changed only slightly with cycling; however, the size of the low-frequency semi-circle increased with cycling. Among the materials, R_{ct} of Sulfate increased slightly during cycling and showed the lowest resistance, 25 Ω, corresponding to the discharge capacity retention results, which can be attributed to a well-ordered layered structure and nano-sized channels that allow contact to carbon black for electric conductivity. R_{ct} of Acetate was 28 Ω for the initial 20 cycles and 29 Ω after 100 cycles. Although the R_{ct} at both 20 and 100 cycles were almost the same, the R_f increased by 5 Ω, which can be attributed to undesirable cation mixing blocking Li^+ ion migration inside the particles. The R_{ct} of Nitrate was 25 Ω for the initial 20 cycles and 63 Ω after 100 cycles. During cycling, the R_{ct} of Nitrate continued to rapidly increase and was larger than Sulfate or Acetate after 100 cycles. This result is due to poor contact with carbon black for electric conductivity and poorer mobility of Li^+ ions because of a lack of channels.

There are various reasons for the deterioration of cycling ability of $LiNi_{0.6}Co_{0.2}Mn_{0.2}O_2$ materials. A major reason for the capacity fading of $LiMO_2$ (M = Ni, Co, Mn) is structural changes during charge/discharge cycling, i.e., an irreversible change from a layered phase to a spinel phase, which can block Li^+ ion intercalation/deintercalation [31]. Another reason is void-channel effects on the surface between the electrode and electrolyte, which can affect the solid electrolyte interphase layer, the contact area of conductive agent, and the mobility of Li^+ ions. To explain why Sulfate had excellent electrochemical properties compared to the other materials, schematic design is developed as shown in Fig. 7. Sulfate had void-channels on the surface of secondary particles formed by agglomeration of primary particles. There are three advantages to the presence of void-channels on the surface, which lead to excellent electrochemical properties. First, particles with void-channels have a more substantial solid electrolyte interphase layer, which protects the material from unexpected reactions and helps transport lithium ions via channels on the surface. Second, electric conductivity grows with increasing contact of the conducting additive carbon black with the surface of cathode active materials in the channels, which can reduce activation polarization at a high C-rate by rapidly moving electrons. Third, Li ions are small-sized particles and void-channels provide easier access to and from the center of particles and the electrolyte avoiding undesirable collisions in the structure.

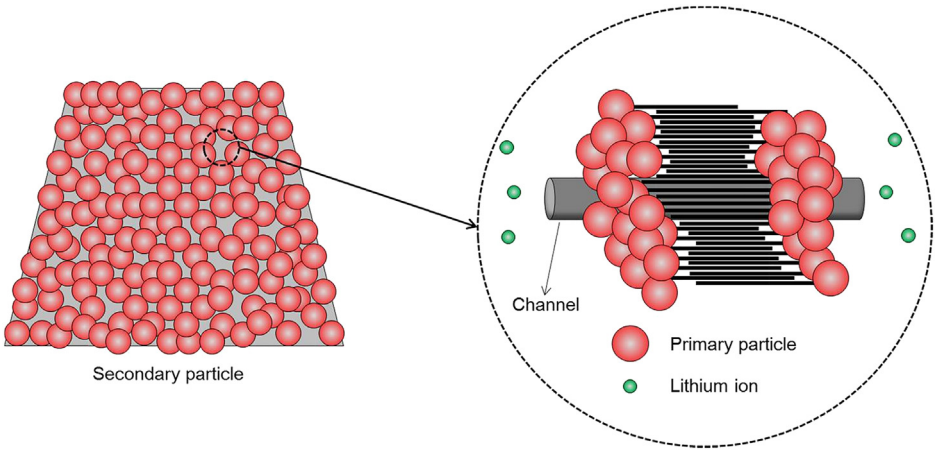

Fig. 7. Schematic design of the effects on void-channels for $Li[Ni_{0.6}Co_{0.2}Mn_{0.2}]O_2$ samples.

4. Conclusion

$Li[Ni_{0.6}Co_{0.2}Mn_{0.2}]O_2$ cathode materials are synthesized using sulfate, nitrate, and acetate inorganic salt starting materials. Secondary particles of Sulfate and Acetate with void channels are formed by agglomeration of nano-sized primary particles, whereas Nitrate has no void channels. Sulfate with void channels and a regular layered structure displays the best electrochemical performances at 1 C- and 6 C-rates. The presence of void channels reduces resistance in the transport of Li-ions to the inside of cathode active materials because an increased surface area with electrolyte provides increased contact with conductive agents. Having a good layered structure prevents cation mixing and allows Li ions to diffuse easily inside the cathode active material. For these reasons, the discharge capacity retention of Sulfate is the highest with 83.2% at 6 C-rate after 100 cycles, although the discharge capacity decreases gradually for the initial 40 cycles. The synthesized cathode active materials like Sulfate are potentially useful for applications involving HEV, P-HEV, EV, and ESS equipped with quick charge–discharge process.

Acknowledgments

This work was supported by the IT R&D program of MOTIE (Ministry of Trade, Industry & Energy)/KEIT (Korea Evaluation Institute of Industrial Technology) [10041856].

References

[1] Y.-S. He, Z.-F. Ma, Y. Jiang, J. Power Sources 163 (2007) 1053–1058.
[2] H.-S. Kim, S.-I. Kim, C.-W. Lee, S.-I. Moon, J. Electroceram. 17 (2006) 673–677.
[3] Y.-K. Sun, D.-H. Kim, H.-G. Jung, S.-T. Myung, K. Amine, Electrochim. Acta 55 (2010) 8621–8627.
[4] H. Konishi, T. Yuasa, M. Yoshikawa, J. Power Sources 196 (2011) 6884–6888.
[5] H. Yoshizawa, M. Ikoma, J. Power Sources 146 (2005) 121–124.
[6] K.-S. Lee, S.-T. Myung, Y.-K. Sun, J. Power Sources 195 (2010) 6043–6048.
[7] L. Wang, J. Li, X. He, W. Pu, C. Wan, C. Jiang, J. Solid State Electrochem. 13 (2009) 1157–1164.
[8] K. Vediappan, S.-J. Park, H.-S. Kim, C.W. Lee, J. Nanosci. Nanotechnol. 11 (2011) 865–870.
[9] H. Arai, S. Okada, Y. Sakurai, J.-I. Yamaki, Solid State Ionics 109 (1998) 295–302.
[10] J. Choi, A. Manthiram, J. Power Sources 162 (2006) 667–672.
[11] Y.-K. Sun, S.-T. Myung, M.-H. Kim, J. Prakash, K. Amine, J. Am. Chem. Soc. 127 (2005) 13411–13418.
[12] Y.-K. Sun, S.-T. Myung, B.-C. Park, J. Prakash, I. Belharouak, K. Amine, Nat. Mater. 8 (2009) 320–324.
[13] M.-H. Lee, Y.-J. Kang, S.-T. Myung, Y.-K. Sun, Electrochim. Acta 50 (2004) 939–948.
[14] Z. Lu, D.D. MacNeil, J.R. Dahn, Electrochem. Solid-State Lett. 4 (2001) A191–A194.
[15] P.S. Whitfield, I.J. Davidson, L.M.D. Cranswick, I.P. Swainson, P.W. Stephens, Solid State Ionics 176 (2005) 463–471.
[16] N. Yabuuchi, T. Ohzuku, J. Power Sources 119–121 (2003) 171–174.
[17] Z. Chang, Z. Chen, F. Wu, X.-Z. Yuan, H. Wang, Electrochim. Acta 54 (2009) 6529–6535.
[18] T.H. Cho, S.M. Park, M. Yoshio, T. Hirai, Y. Hideshima, J. Power Sources 142 (2005) 306–312.
[19] N. Wang, C. Hsu, L. Zhu, S. Tseng, J.-P. Hsu, J. Colloid Interface Sci. 407 (2013) 22–28.
[20] W.-S. Cho, F. Thielbeer, R. Duffin, E.M.V. Johansson, I.L. Megson, W. MacNee, M. Bradley, K. Donaldson, Nanotoxicology 8 (2014) 202–211.
[21] I.S. Bouhaik, P. Leroy, P. Ollivier, M. Azaroual, L. Mercury, J. Colloid Interface Sci. 406 (2013) 75–85.
[22] K.S. Park, M.H. Cho, S.J. Jin, K.S. Nahm, Electrochem. Solid-State Lett. 7 (2004) A239–A241.
[23] J.-H. Ju, K.-S. Ryu, J. Alloys Compd. 509 (2011) 7985–7992.
[24] Y. Sun, C. Ouyang, Z. Wnag, X. Huang, L. Chen, J. Electrochem. Soc. 151 (2004) A504–A508.
[25] H. Liu, Y. Yang, J. Zhang, J. Power Sources 162 (2006) 644–650.
[26] A.W. Moses, H.G.G. Flores, J.-G. Kim, M.A. Langell, Appl. Surf. Sci. 253 (2007) 4782–4791.
[27] J. Li, L. Wang, Q. Zhang, X. He, J. Power Sources 189 (2009) 28–33.
[28] K.M. Shaju, G.V. Subba Rao, B.V.R. Chowdari, J. Electrochem. Soc. 151 (2004) A1324–A1332.
[29] Y.-J. Shin, W.-J. Choi, Y.-S. Hong, S. Yoon, K.S. Ryu, S.H. Chang, Solid State Ionics 177 (2006) 515–521.
[30] Y.S. Yun, J.H. Kim, S.-Y. Lee, E.-G. Shim, D.-W. Kim, J. Power Sources 196 (2011) 6750–6755.
[31] G. Vitins, K. West, J. Electrochem. Soc. 144 (1997) 2587–2592.
[32] M.Z.-C. Hu, G.A. Miller, E.A. Payzant, C.J. Rawn, J. Mater. Sci. 35 (2000) 2927–2936.
[33] V.G. Plekhanov, J. Mater. Sci. 38 (2003) 3341–3429.
[34] C.B. Murray, D.J. Norris, M.G. Bawendi, J. Am. Chem. Soc. 115 (1993) 8706–8715.